Remote control of CAR T cell therapies by thermal targeting

Ian C. Miller[1], Lee-Kai Sun[1], Adrian M. Harris[1], Lena Gamboa[1], Ali Zamat[1] & Gabriel A. Kwong[1–5,*]

[1] *The Wallace H. Coulter Department of Biomedical Engineering, Georgia Institute of Technology & Emory University, Atlanta, GA 30332, USA*

[2] *Institute for Electronics and Nanotechnology, Georgia Institute of Technology, Atlanta, GA 30332, USA*

[3] *Parker H. Petit Institute of Bioengineering and Bioscience, Georgia Institute of Technology, Atlanta, GA 30332, USA*

[4] *Integrated Cancer Research Center, Georgia Institute of Technology, Atlanta, GA 30332, USA*

[5] *Georgia Immunoengineering Consortium, Emory University and Georgia Institute of Technology, Atlanta, GA 30332, USA*

* Corresponding Author: Gabe A. Kwong
Address: Marcus Nanotechnology Building, 345 Ferst Drive, Atlanta, GA 30332, USA
Phone: 404-385-3746
Email: gkwong@gatech.edu

ABSTRACT

The limited ability to control anti-tumor activity within tumor sites contributes to poor CAR T cell responses against solid malignancies. Systemic delivery of biologic drugs such as cytokines can augment CAR T cell activity despite off-target toxicity in healthy tissues that narrow their therapeutic window. Here we develop a platform for remote control of CAR T therapies by thermal targeting. To enable CAR T cells to respond to heat, we construct synthetic thermal gene switches that trigger expression of transgenes in response to mild elevations in local temperature (40–42 °C) but not to orthogonal cellular stresses such as

hypoxia. We show that short pulses of heat (15–30 min) lead to more than 60-fold increases in gene expression without affecting key T cell functions including proliferation, migration, and cytotoxicity. We demonstrate thermal control of broad classes of immunostimulatory agents including CARs, Bispecific T cell Engagers (BiTEs), and cytokine superagonists to enhance proliferation and cell targeting. In mouse models of adoptive transfer, photothermal targeting of intratumoral CAR T cells to control the production of an IL-15 superagonist significantly enhances anti-tumor activity and overall survival. We envision that thermal targeting could improve the safety and efficacy of next-generation therapies by allowing remote control of CAR T cell activity.

INTRODUCTION

Engineered T cell therapies such as Chimeric Antigen Receptor (CAR) T cells are transforming clinical care for hematological malignancies, spurring numerous efforts to expand their use for different cancer types and applications. However, this success has not reliably translated to solid tumors[1]. The factors that contribute to low response rates are multifaceted and include the paucity of tumor-specific antigens, inefficient persistence and expansion of adoptively transferred T cells, and immunosuppression by the tumor microenvironment (TME)[2]. Promising approaches to improve anti-tumor activity of engineered T cells include systemic administration of potent immunostimulatory agents such as cytokines, checkpoint blockade inhibitor antibodies, and bispecific T cell engagers (BiTEs)[3-6]. However, these biologics lack specificity, activate both engineered and endogenous immune cells, and exhibit toxicity in healthy tissue which limits maximum tolerable doses and narrows their therapeutic windows[7-10]. Thus, expanding current abilities to target and locally augment CAR T cell functions at tumor and disease sites such as draining lymph nodes could improve the safety and efficacy of cell-based therapies.

Emerging strategies to control engineered T cells and augment their anti-tumor activity include the use of biomaterials to co-deliver adjuvants to the TME as well as genetic constructs for autonomous expression of immunostimulatory genes. For example, implantation of biopolymer scaffolds loaded with tumor-specific T cells and immunostimulatory adjuvants at the surgical site improved postoperative responses following primary tumor resection in mouse models[11, 12]. To provide a localized source of adjuvants, T cells tethered on their cell surface to nanoparticle 'backpacks' allowed infiltrating T cells to carry cargo[13] and release a one-time dose of drug within tumors[14]. Increasingly sophisticated genetic circuitry has also allowed T cells to locally produce biologics to overcome immunosuppression or target antigens after tumor infiltration. For example, 'armored CARs' leverage constitutive expression of biologics such as IL-12[15], αPD-1 scFvs[16], and BiTEs[17] to improve anti-tumor activity. T cells have also been engineered with sense-and-respond biocircuits that conditionally activate in the presence of specific input signals. These strategies include NFAT-inducible cassettes that upregulate expression of cytokines following T cell recognition of a tumor-associated antigen[18-20]. To further increase specificity, T cells have been engineered to target unique combinations of epitopes expressed in the TME to allow discrimination from healthy cells expressing a single epitope[21]. Such approaches based on Boolean logic require the presence of both target antigens for T cell activation to occur and have demonstrated efficacy in multiple models of focal tumors[22, 23]. Collectively, these approaches illustrate the need to develop strategies to control and improve intratumoral T cell activity.

Here we developed a platform for remote thermal control of CAR T cell therapies. Heat treatments are used clinically to sensitize cancer cells to chemotherapy, ablate isolated metastatic nodules, and enhance diffusion of small molecule drugs into tumors[24]. Both superficial and deep-seeded tumors can be targeted for thermal treatment by platforms including high intensity focused ultrasound (HIFU)[25], laser interstitial thermal therapy (LITT)[26], and electromagnetic heating[27]. To engineer T cells with the ability to respond to heat, we constructed and screened panels of
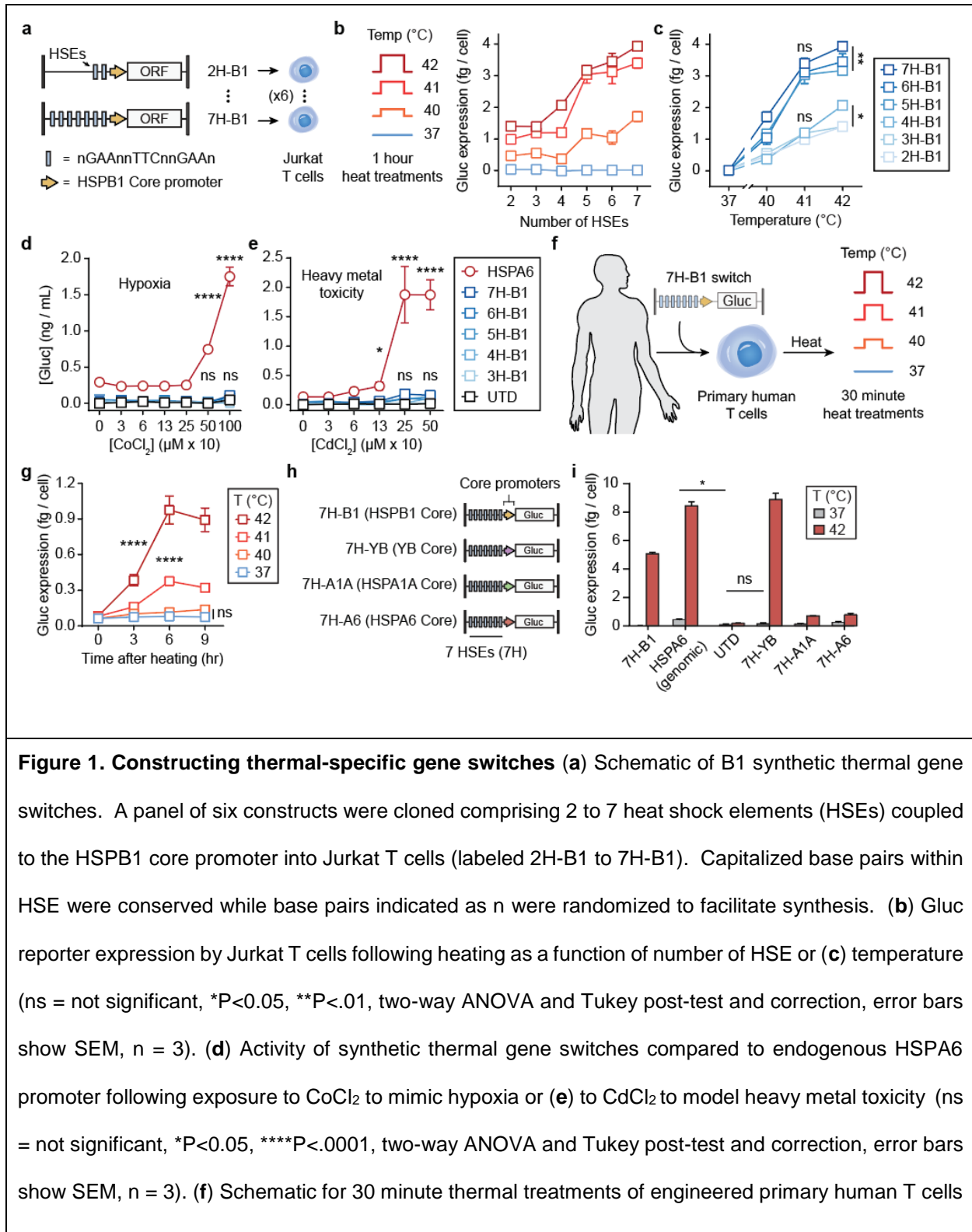
synthetic thermal gene switches containing combinations of Heat Shock Elements (HSEs) and core promoters to identify an architecture that responds to mild hyperthermia while remaining non-responsive to orthogonal cell stresses. We designed thermal constructs to control broad classes of immunostimulatory genes including CARs, BiTEs, and a cytokine superagonist to enhance key T cell functions including proliferation and T cell targeting. In an adoptive transfer model of cancer, remote thermal control of an IL-15 superagonist improved anti-tumor CAR T cell activity by reducing tumor burden and improving survival of tumor-bearing animals. Remote control of CAR T cells by thermal targeting could improve the precision of cellular therapies by enabling site-specific control of anti-tumor responses.

RESULTS

Engineering thermal-specific gene switches

The cellular response to hyperthermia is mediated by trimerization of the temperature-sensitive transcription factor Heat Shock Factor 1 (HSF1) and its subsequent binding to DNA motifs termed Heat Shock Elements (HSEs). HSEs are comprised of multiple inverted repeats of the consensus sequence 5'-nGAAn-3'[28, 29] and are arrayed upstream of HSPs thereby enabling their upregulation following thermal stress[30]. The response of endogenous HSP genes is selective, but not specific, for heat as their promoters contain additional regulatory elements (e.g., hypoxia response elements[31], metal-responsive elements[32]) that mediate transcription following exposure to a diverse set of cues including hypoxia[33], heavy metals[34], and mechanical force[35]. Moreover, differences in the core promoter (e.g., initiator elements, TATA box) influence the composition of the pre-initiation complex (PIC) and its interactions with transcriptional enhancers including HSF1, providing an additional mechanism whereby transcriptional responses to heat are regulated differently across tissues and types of cells[36, 37]. Due to this complexity and cross-activation of

HSP promoters by non-thermal response pathways, we sought to build synthetic gene switches that are activated by heat but not by other sources of stress.

Figure 1. Constructing thermal-specific gene switches (**a**) Schematic of B1 synthetic thermal gene switches. A panel of six constructs were cloned comprising 2 to 7 heat shock elements (HSEs) coupled to the HSPB1 core promoter into Jurkat T cells (labeled 2H-B1 to 7H-B1). Capitalized base pairs within HSE were conserved while base pairs indicated as n were randomized to facilitate synthesis. (**b**) Gluc reporter expression by Jurkat T cells following heating as a function of number of HSE or (**c**) temperature (ns = not significant, *P<0.05, **P<.01, two-way ANOVA and Tukey post-test and correction, error bars show SEM, n = 3). (**d**) Activity of synthetic thermal gene switches compared to endogenous HSPA6 promoter following exposure to $CoCl_2$ to mimic hypoxia or (**e**) to $CdCl_2$ to model heavy metal toxicity (ns = not significant, *P<0.05, ****P<.0001, two-way ANOVA and Tukey post-test and correction, error bars show SEM, n = 3). (**f**) Schematic for 30 minute thermal treatments of engineered primary human T cells

at treatments ranging from 37 to 42 °C. (**g**) Kinetics gluc reporter expression by primary human T cells following heat treatments at indicated temperatures (****P<.0001, two-way ANOVA and Tukey post-test and correction, error bars show SEM, n = 3). (**h**) Schematic of core promoter screen using 7 HSE repeats. (**i**) Activity of thermal gene switches containing different core promoter constructs following heat treatments in primary human T cells (ns = not significant, *P<0.05, one-way ANOVA and Tukey post-test and correction, error bars show SEM, n = 3).

To design thermal-specific gene switches, we cloned 6 candidate constructs comprised of 2 to 7 repeats of the HSE motif 5'-nGAAnnTTCnnGAAn-3' upstream of the Hspb1 core promoter into Jurkat T cells (labeled 2H-B1 to 7H-B1, **Fig. 1a**). We initially selected the Hspb1 core promoter as its parent gene was one of two that were upregulated by more than 20-fold at 42 °C in primary murine T cells in contrast to more than 80 HSP and HSP-related genes that did not respond to heat treatment (**Fig. S1**). We reasoned that by selecting a core promoter from an endogenous gene with a high thermal response, it would facilitate transcriptional activity when integrated with HSE repeats. To quantify responses of our thermal switches, transduced Jurkat T cells were transiently heated to 3–5 °C above body temperature (i.e., 40–42 °C), a mild temperature range in contrast to those used for ablative therapies (>50 °C)[25]. Compared to control samples at 37 °C, we observed increased expression of the reporter Gaussia luciferase (Gluc) as the temperature and number of HSEs increased (**Fig. 1b**). Constructs containing 5–7 HSE repeats (5H-B1 to 7H-B1) resulted in significantly higher thermal response compared to those with 2–4 HSEs (2H-B1 to 4H-B1) (**Fig. 1c**). Collectively, these data confirmed that our synthetic thermal gene switches were heat-sensitive and that the magnitude of the response was dependent on HSE number.

We next tested thermal specificity using hypoxia and heavy metal toxicity as two representative non-thermal stresses[38-40]. As a benchmark, we compared with the endogenous HSPA6 promoter, which is a highly stress-inducible HSP promoter[41] previously used for thermal

control of gene expression[42-45]. We tested the gene switches by incubating transduced Jurkat T cells with the hypoxia-mimetic agent $CoCl_2$ – a stabilizer of the hypoxia response's master regulator Hypoxia Inducible Factor-1α (Hif-1α)[46] – as well as the heavy metal complex cadmium chloride ($CdCl_2$). Whereas Jurkat T cells cloned with the HSPA6 promoter showed dose-dependent activation by hypoxia (**Fig. 1d**) and cadmium toxicity (**Fig. 1e**), T cells transduced with our synthetic gene switches (3H-B1 to 7H-B1) were not activated and remained statistically identical to untransduced (UTD) controls up to concentrations above the ranges commonly used to test cellular responses to hypoxia and cadmium[46-49] (1000 μM $CoCl_2$ and 500 μM $CdCl_2$) (**Fig. 1d**, **e**). These results confirmed that our synthetic gene switches have increased thermal-specificity compared to endogenous HSPs and are not cross-activated when exposed to non-thermal stresses.

To test whether these constructs work in primary human T cells, we transduced T cells with the 7H-B1 thermal switch (**Fig. 1f**). Above a threshold temperature of 40 °C, we observed thermal switch activation that peaked between 3 to 6 hours after heating but was ~40% less responsive compared to the endogenous HSPA6 (**Fig. 1g,h**). Because the Hspb1 core promoter was initially selected from a screen of murine T cells, we reasoned that thermal responses in primary human T cells may be further tuned with different core promoters. Thus, we compared additional core promoters including ones cloned from the HSPA1A gene identified in the qPCR screen (**Fig. S1**), the human HSPA6 gene, and a synthetic core promoter (YB) described previously[50, 51] (**Fig. 1h**). Consistent with our previous observations, we observed negligible activation with heat treatments at 37–40 °C for 24 hours across all 4 constructs tested (**Fig. S2**). By contrast, after 30 minutes at 42 °C, the 7H-YB construct produced the highest Gluc reporter levels while maintaining statistically identical basal activity at 37 °C compared to untransduced controls. This corresponded to a ~60-fold increase in thermal switch activity compared to ~20-fold increases by the endogenous HSPA6 (**Fig. 1i**). On the basis of these data, we selected 7H-YB for subsequent experiments due to its improved thermal specificity and high thermal response.

Primary T cells maintain key functions after thermal treatments

Next, we sought to identify the range of thermal delivery profiles that would be well-tolerated by primary T cells without affecting key functions including proliferation, migration, and cytotoxicity. In thermal medicine, heating target sites to temperatures greater than 50 °C is used to locally ablate tissue by inducing tumor cell apoptosis and coagulative necrosis[25]. By contrast, mild hyperthermia therapy (40–42 °C) is used to enhance transport of small molecules such as in Hyperthermic Intraperitoneal Chemotherapy (HIPEC) where abdominal infusions of heated chemotherapy serve as adjuvant treatment following surgical debulking in advanced ovarian cancer patients[24, 52, 53]. At temperatures below 45 °C, transient exposure to mild hyperthermia is well-tolerated by cells and tissues due to induction of stress-response pathways including HSPs[54]. In addition to temperature range, we also considered T cell responses to continuous and fractionated heat treatments. Dose fractionation is a commonly used approach in radiotherapy to reduce damage to normal tissues[55] while maximizing the effect of radiation on cancer. Based on our previously observations that thermal pulse trains increased Jurkat T cell tolerance compared to continuous heat treatments with an identical treatment area-under-the-curve (AUC)[56], we sought to additionally probe the effect of thermal dose fractionation on primary T cells.

We first compared pulsed heat treatments at 67% duty cycles comprised of three discrete thermal pulses (5 or 10 min each) separated by intervening rest periods at 37 °C (2.5 or 5 min each) to their unfractionated counterparts (15 or 30 min continuous heating) (**Fig. 2a**). Across the conditions tested, we observed significant increases in Gluc reporter expression with pulsed heat treatments at 42 (30 min AUC) and 43 °C (15 and 30 min AUC) by up to ~30% compared to continuous delivery. To assess T cell viability, we quantified death (PI) and apoptotic (Annexin V) markers and observed no significant difference in viability between unheated, pulsed, and continuously heated samples for up to 30 minutes (**Fig. 2b**). By contrast a ~34% reduction in T cell viability was observed in positive control samples that were continuously heat treated for 60 minutes. Similar trends were observed in T cell proliferation assays by dye (CTV) dilution where

the percent of proliferated T cells following incubation with CD3/28 beads was unaffected by both continuous and pulsed heating for 30 minutes at 42 or 43 °C while positive control samples that were heated for 60 minutes resulted in reduced T cell proliferation (**Fig. 2c**).
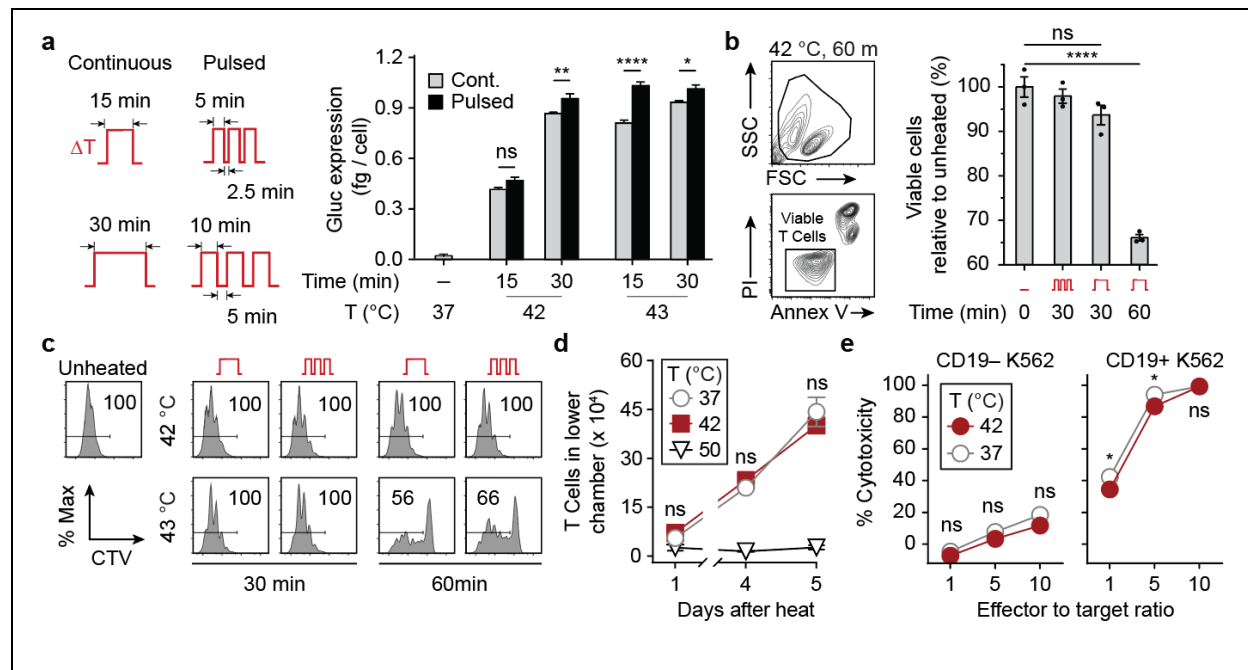
Figure 2. Thermal treatments are well-tolerated by primary human T cells. (**a**) Gluc activity of primary human T cells after continuous (grey) and pulsed (black) heat treatments with temperatures, total durations, and heating profiles as indicated (ns = not significant, *P<0.05, **P<0.01, ****P<0.0001, t-test, error bars show SEM, n = 3). (**b**) Propidium Iodide (PI) and Annexin V flow staining of CD3+ T cells. Bars represent viable populations (PI−Annexin V−) normalized to unheated samples (ns = not significant, ****P<0.0001, one-way ANOVA and Dunnett post-test and correction, error bars show SEM, n = 3). (**c**) CellTrace Violet (CTV) flow histograms of T cells after heat treatments and incubation with CD3/28 beads at a 3:1 bead to T cell ratio. (**d**) Number of cells in lower well of a transwell plate containing CXCL12. T cells were heated and loaded into the top well prior to sampling at indicated timepoints (ns = not significant between 37 °C and 42 °C, two-way ANOVA and Tukey post-test and correction, error bars show SEM, n = 3). (**e**) Percent cytotoxicity observed in CD19− or CD19+ luciferized K562 cells after incubation with T cells constitutively expressing CARs after heating with

effector to target ratios as indicated (ns = not significant, *P<0.05, two-way ANOVA and Sidak post-test

and correction, error bars show SEM, n = 3).

To probe the effects of thermal treatments on T cell migration, we used transwell assays

to assess T cell chemotaxis and observed that heat treatments (42 °C for 30 min) did not

significantly affect T cell migration into lower wells containing the chemokine CXCL12 compared

to unheated controls whereas T cells heated to 50 °C were affected (**Fig. 2d**). To test longitudinal

activation, we re-heated T cells over the course of 8 days and observed similar increases in GFP

mean fluorescent intensity (MFI), as well as GFP activation and decay half-lives ($t_{1/2}$ ~0.5 and 1

day, respectively), suggesting that the magnitude and kinetics of T cell responses are unaffected

by multiple heat treatments (**Fig. S3**). To quantify the effect of heat on T cell cytotoxicity, we

incubated primary human T cells expressing an αCD19 CAR under a constitutive EF1α promoter

with either CD19+ or CD19- K562s containing a luciferase reporter to allow quantification of cell

death by loss of luminescence (**Fig. 2e**). At all effector to target cell ratios tested (1:1, 5:1, 10:1),

heated T cells maintained greater than 90% of the cytotoxicity observed in unheated samples

while no significant difference in cytotoxicity was observed in samples containing CD19- K562

target cells (**Fig. 2e**). Collectively, these data demonstrate that primary human T cells maintain

the ability to proliferate, migrate, and kill target cells following short heat treatments delivered in

continuous or pulsed wave forms for less than 30 minutes in duration.

Thermal control of CAR T cell functions

The factors that contribute to durable anti-tumor responses include the degree to which key steps

in the immunity cycle can be effectively directed against tumors[57]. Here we sought to build thermal

circuitry to allow control over key CAR T functions including proliferation, antigen recognition, and

T cell killing. We first explored thermal control of CAR T cell killing where the expression of an

αCD19 CAR was placed under control of a thermal switch (TS-CAR) (**Fig. 3a**). Following heat treatment, TS-CAR T cells expressed αCD19 CARs to levels comparable to control T cells transduced with a constitutive vector (EF1α-CAR) (**Fig. 3b**). To test heat-triggered control of cytotoxicity, we heated TS-CAR T cells across a range of activation temperatures (40, 41, and 42 °C) and incubated them with either CD19– or CD19+ K562 target cells. We observed that intracellular Granzyme B levels – a cytotoxic effector molecule released by T cells – increased in CD19+ target cells as a function of temperature in contrast to control cells that lacked the CAR antigen (**Fig. 3c**). This was further supported by a TS-CAR T cell killing assay where we observed significant increases in CD19+ K562 cell death as the T effector to target cell ratio was increased following thermal treatments at 42 °C (**Fig. 3d**).
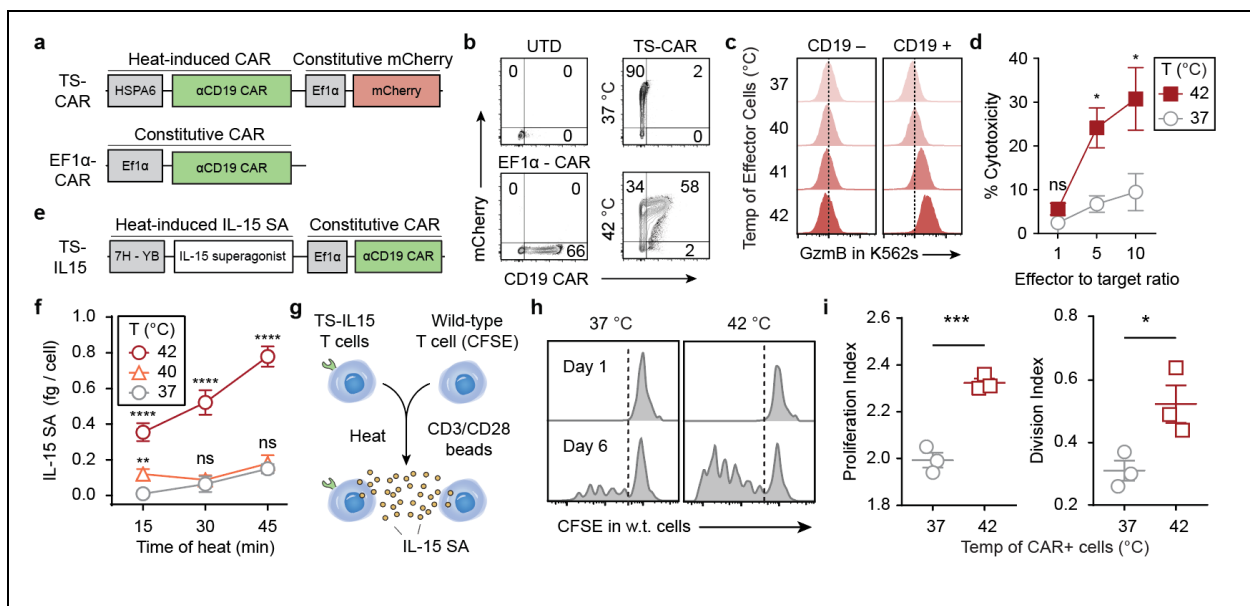

Figure 3. Thermal control of CAR T cell effector functions. (**a**) Schematic of a heat-inducible TS-CAR and constitutive EF1α CAR construct. (**b**) CAR flow staining with biotinylated CD19 on UTD, constitutive, and TS-CAR T cells. (**c**) Intracellular Granzyme B staining in K562 target cells after incubation with heated TS-CAR T cells. K562s lacking CAR antigen graphed in left column while CD19+ K562s are displayed in right column. (**d**) Killing of target CD19+ K562 cells by TS-CAR T cells (ns = not significant, *P<0.05, two-way ANOVA and Tukey post-test and correction, error bars show

SEM, n = 3). (**e**) Schematic of TS-IL15 construct containing heat-triggered IL-15 superagonist and a constitutive CAR. (**f**) IL-15 superagonist concentrations in supernatant of TS-IL15 T cells following heat treatments. Temperature and duration of treatments are as indicated (ns = not significant, **P<0.01, ****P<0.0001, two-way ANOVA and Tukey post-test and correction, error bars show SEM, n = 3, comparisons are to unheated control). (**g**) Experimental design for co-culture assay of TS-IL15 cells and CFSE-labeled wild-type cells. CD3/28 beads were added at 1:10 bead to T cell ratio. (**h**) Representative flow histograms and (**i**) quantified proliferation and division indices as calculated by FlowJo proliferation tool of the CFSE-labeled wild-type T cell population (*P<0.05, t-test).

We further sought to determine whether thermal control could enhance T cell activation and proliferation. To do this, we cloned a single-chain IL-15 superagonist (IL-15 SA) comprised of the cytokine tethered to the sushi domain of the IL-15Rα subunit[58] under control of our thermal vector (TS-IL15). IL-15 SAs are potent stimulants of CD8 T cells and NK cells and a clinical candidate, ALT-803, is currently under investigation for a wide range of cancers[59, 60]. To verify heat-triggered secretion of IL-15 SA, we analyzed conditioned media by ELISA and found that IL-15 SA levels increased with the duration and temperature of thermal treatment (**Fig. 3f**). To test whether heat-induced IL-15 SA was functionally active, we developed a T cell proliferation assay using CFSE-labeled wild-type T cells incubated with CD3/28 beads at a 10:1 ratio without supplemental cytokines. We found that this condition was insufficient to induce T cell proliferation compared to conditions when cytokines such as IL-2 was present in media (**Fig. S4**). Therefore, to test thermal control of IL-15 SA, we added heated or unheated TS-IL15 T cells to samples containing CFSE-labeled wild-type T cells with CD3/28 beads at a 10:1 T cell to bead ratio (**Fig. 3g**). Compared to unheated controls, we found that CFSE-labeled T cells in heated samples expanded with significantly higher proliferation and division indices (**Fig. 3h, i**), demonstrating that TS-IL15 T cells are capable of producing physiologically active levels of IL-15 SA following a single thermal treatment.

Last, we explored thermal control to expand CAR T recognition of tumor-associated antigens to include NKG2D ligands (NKG2DLs), which are upregulated on a wide range of cancers as well as suppressor cells[61-64]. Targeting NKG2DLs is limited by their expression in healthy cells such as intestinal epithelial cells and bone marrow stromal cells[65]. To enable thermal control of CAR T cells to target NKG2DL+ cells, we cloned a previously described NKG2DL-BiTE containing CD3-recognition domains from the OKT3 antibody linked to the extracellular domain of the human NKG2D receptor[64]. Our vector (TS-BiTE) included an Igκ leader sequence for BiTE secretion, a HisTag reporter, and a constitutive αCD19 CAR (**Fig. 4a**). After heat treatment, we observed that TS-BiTE Jurkat T cells were stained positively on the cell surface by anti-HisTag antibodies compared to control cells transduced with a Fluc reporter vector (TS-Fluc) (**Fig. 4b**). Based on this, we postulated that T cells would activate by local BiTE binding to CD3 expressed by the same T cell (i.e., autocrine activation) before additional BiTEs would engage bystander T cells (i.e., paracrine activation). To test this, we heated a mixture of TS-BiTE transduced Jurkat T cells (i.e., CAR+) with untransduced cells (i.e., CAR-) as bystanders prior to co-incubation with NKG2DL+ CD19- K562 target cells (**Fig 4c–e**). This experimental setup allowed us to isolate T cell activation based on BiTE engagement without confounding factors due to CD19 CAR binding. We found that expression of the early activation marker CD69 on TS-BiTE Jurkat T cells was significantly upregulated compared to bystander cells as heating durations were extended (red versus black) (**Fig. 4f, g**). By contrast, CD69 was minimally upregulated on bystander cells compared to untransduced Jurkat T cells that were incubated with K562 cells and heated in separate wells as controls (black versus gray). These data provided support that TS-BiTE T cells are primarily activated to target NKG2D ligands in an autocrine path. Finally, to quantify cytotoxicity from heat-triggered expression of BiTEs, we co-incubated primary human TS-BiTE T cells with NKG2DL+ CD19- K562 cells. In contrast to untransduced (UTD) or TS-Fluc controls, TS-BiTE T cells secreted increasing levels of T_h1 cytokines IFN-γ and TNF-α as temperatures were raised from 37 to 42 °C (**Fig. 4h**). We also observed temperature-dependent increases in

K562 cytotoxicity but not at 37 °C compared to UTD controls, demonstrating lack of BiTE-induced killing at basal temperatures (**Fig. 4i**). Taken together, our data showed that thermal control can be extended to broad classes of immunomodulatory molecules to direct CAR T cell functions including proliferation, targeting, and cytotoxicity.
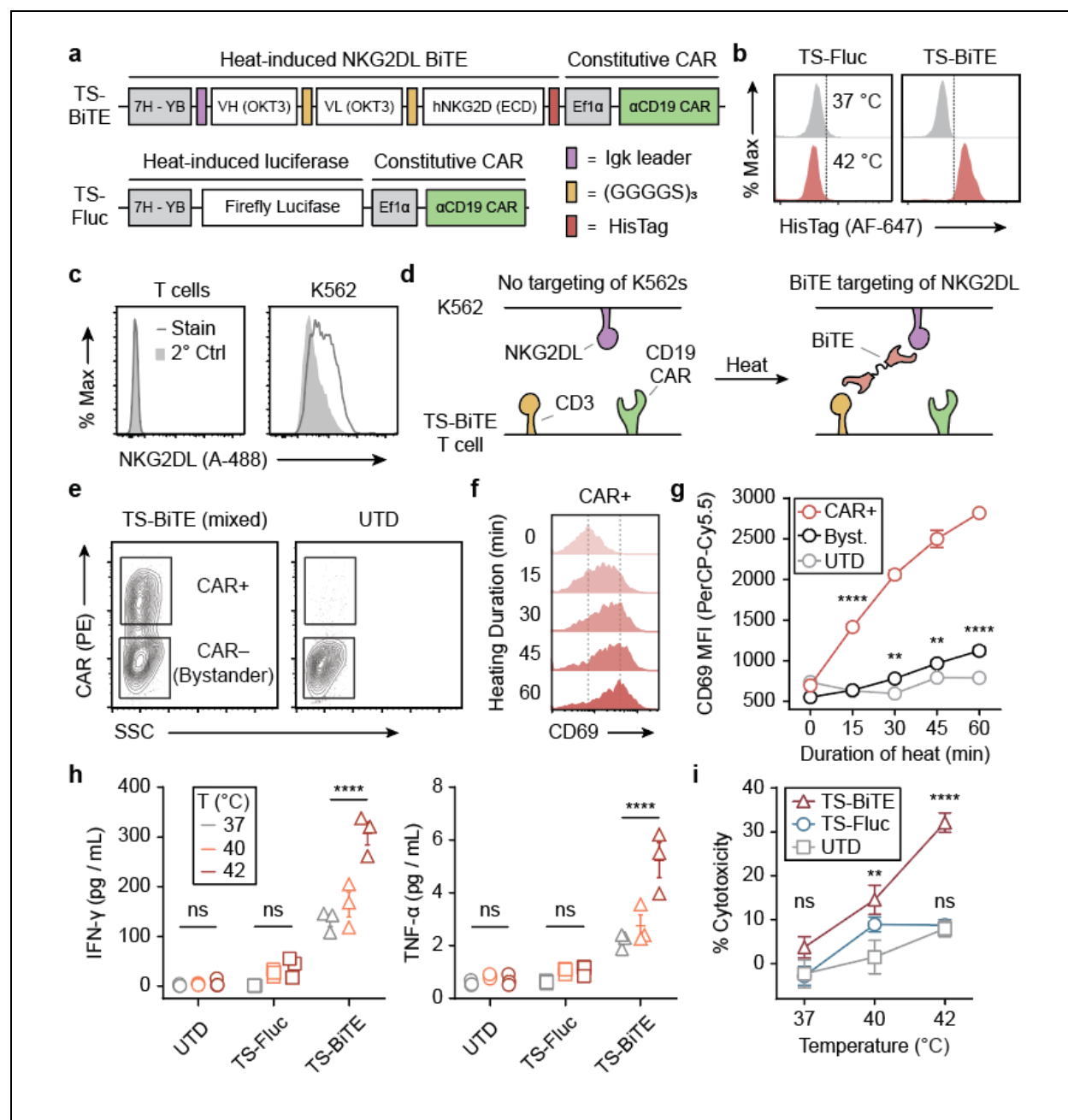
Figure 4. Expanding CAR T cell targeting via heat-triggered BiTEs (**a**) Schematic of TS-BiTE and TS-Fluc thermal switches containing heat-triggered transgenes and constitutive CARs. (**b**) Histograms for HisTag staining in TS-BiTE and TS-Fluc primary T cells following heating. (**c**) NKG2DL staining on primary human T cells and K562s using an NKG2D-Fc chimera and an αFc-A488 secondary antibody. Stain = full staining, 2° Ctrl = secondary antibody only. (**d**) Schematic depicting BiTE-mediated targeting of K562 target cells lacking the CAR target antigen via BiTE binding to NKG2DL and CD3. (**e**) Gating strategy for defining bystander cells based on CD19 CAR expression in Jurkat co-culture assays with K562s. UTD controls were gated on the lower (CAR-) population for graphing in (**g**). (**f, g**) Expression of CD69 on Jurkat T cells following heating and incubation with K562s. TS-BiTE CAR+ histograms (**f**) and summary data of indicated populations (**g**) are graphed, (stats show comparison to UTD, ns = not significant, **P<0.01, ****P<0.0001, two-way ANOVA and Tukey post-test and correction, error bars show SEM, n = 3). (**h**) Cytokine concentrations in supernatant of primary human T cells containing indicated thermal switches after heat treatments and incubation with K562 cells, (ns = not significant, ****P<0.0001, two-way ANOVA and Tukey post-test and correction, error bars show SEM, n = 3). (**i**) Cytotoxicity against K562s as quantified by luciferase assay after incubation with primary human T cells containing the indicated thermal switches, (ns = not significant, **P<0.01, ****P<0.0001, two-way ANOVA and Tukey post-test and correction, comparisons are to UTD control, error bars show SEM, n = 3).

Photothermal targeting of CAR T cells enhances anti-tumor therapy

We next sought to determine whether thermal control of CAR T cells would enhance efficacy of adoptive therapies. To locally heat tumors, we used plasmonic gold nanorods (AuNRs) as antennas to convert incident near infra-red (NIR) light (~650-900 nm) into heat[66]. PEG-coated AuNRs are well-studied nanomaterials with long circulation times that passively accumulate in tumors following intravenous administration[67, 68]. To confirm photothermal heating and thermal switch activation, primary T cells transduced with TS-Fluc were co-incubated with AuNRs in 96-well plates and irradiated with 808 nm laser light. In wells that reached 40–45 °C as monitored by

a thermal camera, we observed a marked increase in luminescent signals when TS-Fluc T cells were present but not in wells containing untransduced controls (**Fig. 5a**), confirming plasmonic photothermal control of engineered T cells.

To implement photothermal targeting in living mice, we inoculated NSG mice with bilateral flank tumors with one cohort receiving CD19– K562 cells and a separate cohort receiving CD19+ Raji cells to model CAR antigen positive and negative tumors (**Fig. 5b-c**). Following intravenous injection of AuNRs and adoptive transfer of T cells with constitutively expressed αCD19 CAR and thermal Fluc (TS-Fluc vector), we irradiated tumors with NIR laser light under the guidance of a thermal camera (**Fig. 5d**) to maintain target skin temperatures (**Fig. 5e**). After 20-minute heat treatments, luminescence was contained within Raji tumors receiving NIR light with Fluc activity upregulated greater than 30-fold at these sites compared to unheated Raji tumors in the same animal (**Fig. 5f**). Similar to *in vitro* experiments, CAR T cells could be repeatedly activated in Raji tumors (**Fig. S5**) but by contrast, we did not observe increased activity within antigen-negative K562 tumors following NIR heating (**Fig. 5f**). We attributed this lack of heat-induced activity to the greater than 20-fold lower density of intratumoral CAR T cells in resected K562 tumors that lack the CD19 CAR antigen (**Fig. S6**). Collectively these data demonstrate that the activity of intratumoral T cells engineered with thermal gene switches can be controlled by localized photothermal heating.

To augment CAR T cell therapies by thermal targeting, we adoptively transferred T cells transduced with TS-IL15 vector into NSG mice bearing CD19+ K562 tumors to allow thermal control of the single-chain IL-15 superagonist by cells constitutively expressing an αCD19 CAR. Photothermal heating of tumors was then carried out every 3-4 days (Days 11, 15, 18, 22, and 25) for a total of five treatments (**Fig. 5h**). Compared to control mice that did not receive CAR T cells or heat treatments (black), thermal treatment of tumor sites alone did not lead to reduction in tumor burden or improvement in survival (gray) (**Fig. 5g–i**). Transfer of TS-IL-15 CAR T cells alone significantly reduced tumor burden and improved survival (blue) yet greater than 70% (5/7)

of animals reached euthanasia criteria within 38 days of ACT. By contrast, ACT of TS-IL15 CAR T cells combined with NIR treatments markedly reduced tumor burden and no animals reached euthanasia criteria within the time window of the study. Together, these data demonstrated that thermal targeting of tumors to control CAR T cell production of an IL-15 superagonist significantly improved tumor control and therapeutic outcomes.
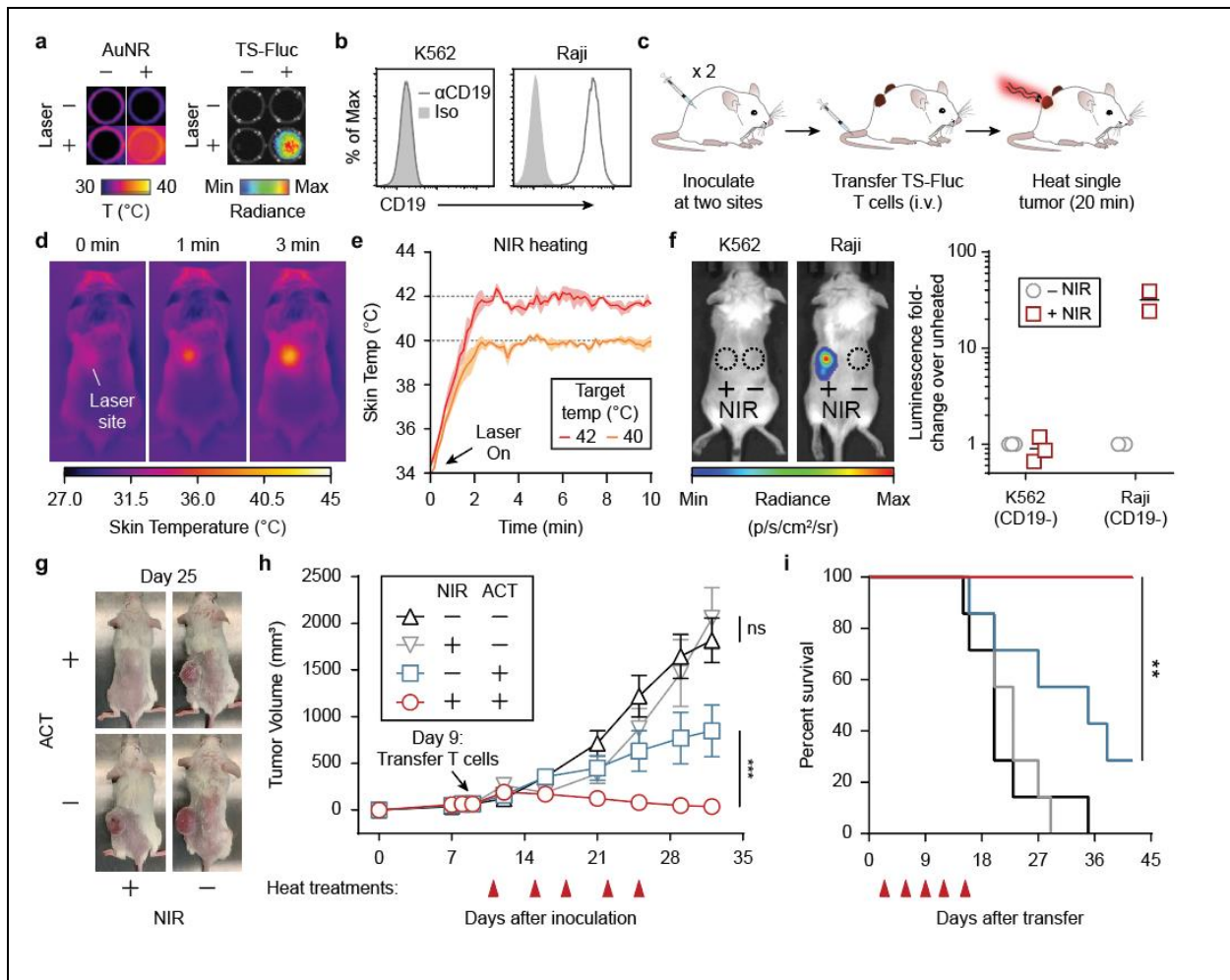
Figure 5. Photothermal targeting of CAR T cells improves anti-tumor responses. (**a**) Thermal and luminescent images of wells containing TS-Fluc T cells after irradiation with NIR laser light. Thermal images were acquired using a FLIR thermal camera while luminescent images were acquired using an IVIS Spectrum CT system (**b**) CD19 staining on K562 and Raji cell lines used for tumor inoculations, Iso = isotype control. (**c**) Schematic for experimental timeline where both flanks of each mouse were

inoculated with the same cell line. TS-Fluc T cells were transferred via intravenous tail-vein injections. (**d**) Serial thermal images of tumor-bearing mouse during laser irradiation, timepoints as indicated. (**e**) Thermal kinetic traces (colored lines) showing average skin temperature of a 3 x 3 pixel ROI centered on laser site targeted on tumor. Shaded regions around traces show standard deviation of 3 heating runs. (**f**) Left: Luminescent images of heated mice bearing either K562 (CD19-) or Raji (CD19+) tumors. Right: Luminescence of each tumor site relative to the luminescence from the unheated tumor in the same animal. ROI's were drawn as indicated in left panel. (**g**) Representative pictures of mice bearing CD19+ K562s on Day 25. (**h**) Tumor growth curves following inoculation of CD19+ K562 T cells on Day 0, transfer of TS-IL15 T cells on Day 9 and heat treatments on Days 11, 15, 18, 22, and 25, (ns = not significant, ***P<0.001, two-way ANOVA and Tukey post-test and correction, error bars show SEM, n = 7). (**i**) Survival curves of tumor-bearing mice in (**g**) and (**h**) following transfer of TS-15 T cells and heat treatments, (**p < .01, Log-rank (Mantel-Cox) test, n = 7).

DISCUSSION

Here we developed a platform for remote thermal control of T cell activity. Remote control of T cells by small-molecules or light[69, 70] either require systemic administration or are limited by light penetration through tissue. By contrast, thermal targeting of tissues can be accomplished by several platforms[25] including focused ultrasound, which was recently demonstrated for control of T cell gene expression[71] or thermal control of bacteria engineered with temperature-sensitive repressors[72]. To provide T cells the capacity to respond to heat, we designed synthetic thermal gene switches comprised of arrays of heat shock elements upstream of a core promoter. This architecture eliminated sensitivity to non-thermal stresses such as hypoxia and its thermal response was tunable based on the number of HSEs or different core promoters. While we tested constructs containing up to 7 HSEs paired with 4 core promoters, future work could explore a larger library of building parts including temperature-sensitive transcription factors such as HSF1

to tune response to heat. Importantly, we observed negligible activation of our thermal gene switches at temperatures ≤ 40 °C even when T cells were incubated for over 24 hours. This provides support that the temperature threshold for activation is higher than the range of typical fevers (~38-40 °C)[73-75] in patients with cytokine release syndrome (CRS), which would prevent T cell activation without a targeted thermal input. Despite this, we envision that the development of future thermal gene switches with lower temperature activation thresholds may be useful as a sense-and-respond circuit to autonomously detect fever temperatures and trigger expression of therapeutic agents such as tocilizumab to attenuate CRS.

With our current platform, we demonstrated thermal control of T cell activity using several classes of immunostimulatory genes including CARs, BiTEs, and cytokines. Engineered T cells that constitutively express similar classes of molecules have demonstrated strong anti-tumor efficacy but their therapeutic applications are limited by off-tumor effects and toxicities in healthy tissues[2, 9, 76, 77]. Thus, targeted expression of these genes within tumors could potentially contain potent T cell activity within the local TME and improve therapeutic outcomes. Given that the classes of molecules we studied included surface receptors, secreted cytokines, and bi-specific T cell engagers, we expect that a wide range of biologics are amenable for thermal control without potential loss of function due to protein misfolding or aggregation in T cells by heat stress. In the future, we anticipate that thermal targeting may have clinical use to treat cancer types that present as primary tumors with limited metastasis such as glioblastoma (GBM) or manage locally disseminated disease such as liver, lung, or brain oligometastases that are currently treated by surgical resection or ablation.

Methods

Plasmid construction. Synthetic thermal switches were produced as gene blocks by IDT and cloned into the Lego-C backbone (Addgene plasmid #27348). The core promoters were truncated immediately upstream of their previously described TATA boxes at their 5'-termini and at their translational start site on their 3'-termini [78-80]. The genomic HSPA6 promoter was amplified from genomic DNA using PCR primers listed in a previous publication[81]. The NKG2DL BiTE sequence

was described previously[64] and modified to include an Igκ leader sequence to facilitate secretion from T cells as well as a HisTag for construct detection. This combined sequence was synthesized (ATUM) and cloned downstream of synthetic thermal switches. The IL-15 superagonist sequence was described previously[58] and synthesized by ATUM without modification. The constitutive αCD19 CAR was kindly provided by Dr. Krishnendu Roy (Georgia Institute of Technology).

Culture of primary human T cells and cell lines. CD19+ K562 and wild-type K562s were acquired from Dr. Yvonne Chen (UCLA). These cell lines were cultured in Isocove's Modified Dulbecco's Medium (ThermoFisher #12440053) supplemented with 10% FBS (Fisher #16140071) and 10 U/ml Penicillin-Streptomycin (Life Technologies #15140-122). Raji cells were obtained from Dr. Krishnendu Roy and cultured in RPMI-1640 media supplemented with 10% FBS. Primary Human CD3+ cells were obtained from an anonymous donor blood after apheresis (AllCells) and were cryopreserved in 90% FBS and 10% DMSO until subsequent use. After thawing, cells were cultured in human T cell media comprised of X-VIVO 10 (Lonza #04-380Q), 5% human AB serum (Valley Biomedical #HP1022), 10 mM N-acetyl L-Cysteine (Sigma #A9165), and 55 µM 2-mercaptoethanol (Sigma #M3148-100ML) supplemented with 50 units/ mL human IL-2 (Sigma #11147528001).

Lentiviral production and primary cell transduction. VSV-G pseudotyped lentivirus was produced via transfection of HEK 293T cells (ATCC) using psPAX2 (Addgene #12260) and pMD2.G (Addgene #12259); viral supernatant was concentrated using PEG-it virus precipitation solution (System Biosciences LV825A-1) according to manufacturer instructions. For viral transductions, primary human T cells were thawed, incubated for 24 hours, and activated with Human T-Activator beads (Life Technologies #11131D) at a 3:1 bead:cell ratio for 24 hours. To transduce the activated T cells, concentrated lentivirus was added to non-TC treated 6-well plates which were coated with retronectin (Takara #T100B) according to manufacturer's instructions and spun at 1200 x g for 90 min at room temperature. Following centrifugation, viral solution was aspirated and 2 mL of human T cells (250,000 cells / mL) in human T cell media containing 100 units / mL hIL-2 were added and spun at 1200 x g for 60 min at 37 °C and moved to an incubator. Cells were incubated on a virus-coated plate for 24 hours prior to expansion and Dynabeads were removed 7 days after T cell activation. For cells flow-sorted prior to adoptive cell transfer, Dynabeads were added immediately after sorting at 3:1 ratios for 48 hours.

Staining and flow cytometry. To detect CAR expression, biotinylated CD19 (10 µg / mL; Acro Biosystems #CD9-H8259) and Streptavidin-APC (ThermoFisher #S868) were used according to manufacturer instructions. NKG2DL expression was assessed by staining with NKG2D-Fc chimera (10 µg / mL; Fisher 1299NK050) followed by an αFc secondary stain (Invitrogen #A-10631). NIR Live/Dead (ThermoFisher #L34976), CFSE (LifeTech #C34554) and CellTrace Violet (CTV; LifeTech #C34557) were used according to manufacturer instructions. Human Fc block (BD #564220) was used prior to staining with any antibodies. For intracellular staining for Granzyme B, intracellular fixation and permeabilization buffers (eBioscience #88-8823-88) were used according to manufacturer instructions with Brefeldin A being added ~4 hours prior to staining. Antibodies for Granzyme B (GB12; ThermoFisher), CD69 (FN50; BD), CD4 (RPA-T4; BioLegend); CD8 (RPA-T8; BioLegend), CD3 (UCHT1; BD), CD45 (HI30; BD), CD19 (HIB19; BioLegend), and HisTags (4E3D10H2/E3; ThermoFisher) were all used at 1:100 dilutions.

In vitro *luciferase and thermotolerance assays.* Primary human T cells were heated in a thermal cycler and transferred to culture plates for incubation at 37°C. Unless otherwise noted, cellular supernatant was sampled for luciferase activity 24 hours after conclusion of thermal treatment. Non-thermal treatments were conducted by incubating engineered cells at indicated concentrations of $CoCl_2$ (Sigma #232696-5G) or $CdCl_2$ (Sigma #202908). When indicated,

luminescence was compared to a ladder of recombinant Gaussia Luciferase (NanoLight #321-500) quantified using a Gaussia Luciferase Glow Assay Kit (ThermoFisher #16161) according to manufacturer's instructions. For viability and proliferation studies, primary human T cells were heated in the thermal cycler prior to assaying with an apoptosis detection kit (BD # 556547) or CellTrace Violet (Fisher # C34571). For migration studies, wild-type cells were added to the top insert of a transwell plate (Sigma #CLS3421) while CXCL12 (50 ng / mL, Peprotech #300-28A) was added to the lower chamber. Cells in lower chamber were counted by hemocytometer at indicated times.

Cytotoxicity and T cell activation assays. For cytometric analysis, TS-CAR T cells were heated in a thermal cycler and co-incubated with K562 target cells at a 10:1 effector cell to target cell ratio for 24 hrs prior to staining as described above. For luciferase-based assays, K562s were luciferized with either Firefly luciferase (CD19+) or Renilla luciferase (CD19-) and incubated with effector cells after heating. Unless otherwise noted, a 10:1 effector to target ratio was used. After incubation, either D-luciferin (Fisher #LUCK-2G; 150 µg / mL read concentration) or Rluc substrate (VWR # PAP1232; 17 µM read concentration). Maximum cytotoxicity was defined as luminescent signal from wells containing only media while no cytotoxicity was defined by wells containing only target cells. Supernatant was collected after incubation and assayed for cytokines using the human Th1/Th2/Th17 CBA kit (BD # 560484). IL-15 superagonist was quantified using the human IL-15/IL-15R alpha complex DuoSet ELISA (R&D Systems DY6924).

IL-15 superagonist Dynabead experiment: Wild-type primary human T cells were labeled with CFSE and incubated with either heated or unheated TS-IL15 cells. Beads were added at a 10:1 T cell to bead ratio that was determined not to induce strong proliferation in untransduced T cells without cytokine support (Fig. S4). CFSE labeling allowed discrimination from TS-IL15 cells and proliferation and division indices were calculated in FlowJo using the Proliferation tool.

Animals: Eight- to sixteen-week old female NSG mice were used for all in vivo experiments. Mice were bred and housed in the Georgia Tech Physiological Research Laboratory (GT PRL) prior to start of experiments. All animal protocols were approved by Georgia Tech IACUC (protocols no. A100190 and 100191). All authors have complied with relevant ethical regulations while conducting this study.

Photothermal heating and in vivo *bioluminescence imaging:* AuNRs were purchased from Nanopartz (# A12-10-808-CTAB-500) and pegylated (Laysam Bio # #MPEG-SH-5000-5g) to replace the CTAB coating. These AuNRs were intravenously injected into tumor-bearing mice (10 mg / kg) ~48 hrs before adoptive transfer of T cells. Mice were anesthetized with isoflurane gas, and target sites were irradiated using an 808 nm laser (Coherent) under guidance of a thermal camera (FLIR model 450sc). Fluc activity was measured using an IVIS Spectrum CT (Perkin Elmer) ~5 minutes after intravenous injections of D-luciferin (Fisher #LUCK-2G).

Adoptive cell transfer (ACT) experiments: NSG mice were inoculated subcutaneously with 5×10^6 Raji or K562 cell lines after the site was shaved and sterilized using an isopropyl wipe (GT PRL). ~48 hrs prior to adoptive transfer of human T cells, pegylated AuNRs were injected intravenously via tail vein. Once tumors had reached ~100-150 mm^3, 1.5×10^6 primary human T cells were injected via tail vein in 200 µL of sterile saline. Cells were transduced and sorted based on CD19 CAR expression prior to transfer as described above. After >24 hrs, photothermal heat treatments were administered and monitored as described above. Tumors were measured using digital calipers and volume calculated based on the equation length x width x depth x 0.52. Mice were euthanized when tumor volume exceeded 1500 mm^3.

Software and Statistical Analysis. All results are presented as mean, and error bars show SEM. Statistical analysis was performed using GraphPad Prism statistical software. For all graphs, * p

< .05, ** p < .01, *** p<.001, **** p<.0001, ns = not significant. Flow cytometry data were analyzed using FlowJo X (FlowJo, LLC). Whole-mouse luminescence data were analyzed using Living Image software (PerkinElmer). Figures were designed in Adobe Illustrator.

Data availability

All data supporting the findings of this study are available within the manuscript and its Supplementary Information. Raw data are available from the corresponding authors.

Acknowledgements

Author Contributions

I.C.M., and G.A.K. conceived of the idea. I.C.M., L.K.S., and G.A.K. designed the experiments and interpreted results. I.C.M. and L.K.S. performed the experiments. I.C.M. and G.A.K. wrote the manuscript.

Competing interests

I.C.M., M.G.C., and G.A.K. are listed as inventors on a patent application pertaining to the results of this paper.

References

1.   Lim, W.A. & June, C.H. The Principles of Engineering Immune Cells to Treat Cancer. *Cell* **168**, 724-740 (2017).
2.   Weber, E.W., Maus, M.V. & Mackall, C.L. The Emerging Landscape of Immune Cell Therapies. *Cell* **181**, 46-62 (2020).
3.   John, L.B. et al. Anti-PD-1 antibody therapy potently enhances the eradication of established tumors by gene-modified T cells. *Clin Cancer Res* **19**, 5636-5646 (2013).
4.   Klebanoff, C.A. et al. IL-15 enhances the in vivo antitumor activity of tumor-reactive CD8+ T cells. *Proc Natl Acad Sci U S A* **101**, 1969-1974 (2004).
5.   John, L.B., Kershaw, M.H. & Darcy, P.K. Blockade of PD-1 immunosuppression boosts CAR T-cell therapy. *Oncoimmunology* **2**, e26286 (2013).
6.   Slaney, C.Y., Wang, P., Darcy, P.K. & Kershaw, M.H. CARs versus BiTEs: A Comparison between T Cell-Redirection Strategies for Cancer Treatment. *Cancer Discov* **8**, 924-934 (2018).
7.   Weber, J.S., Kahler, K.C. & Hauschild, A. Management of immune-related adverse events and kinetics of response with ipilimumab. *J Clin Oncol* **30**, 2691-2697 (2012).
8.   Waldmann, T.A. et al. Safety (toxicity), pharmacokinetics, immunogenicity, and impact on elements of the normal immune system of recombinant human IL-15 in rhesus macaques. *Blood* **117**, 4787-4795 (2011).
9.   Conlon, K.C. et al. Redistribution, hyperproliferation, activation of natural killer cells and CD8 T cells, and cytokine production during first-in-human clinical trial of recombinant human interleukin-15 in patients with cancer. *J Clin Oncol* **33**, 74-82 (2015).
10.   Baumeister, S.H., Freeman, G.J., Dranoff, G. & Sharpe, A.H. Coinhibitory Pathways in Immunotherapy for Cancer. *Annu Rev Immunol* **34**, 539-573 (2016).
11.   Smith, T.T. et al. Biopolymers codelivering engineered T cells and STING agonists can eliminate heterogeneous tumors. *J Clin Invest* **127**, 2176-2191 (2017).
12.   Stephan, S.B. et al. Biopolymer implants enhance the efficacy of adoptive T-cell therapy. *Nat Biotechnol* **33**, 97-101 (2015).
13.   Stephan, M.T., Moon, J.J., Um, S.H., Bershteyn, A. & Irvine, D.J. Therapeutic cell engineering with surface-conjugated synthetic nanoparticles. *Nat Med* **16**, 1035-1041 (2010).
14.   Tang, L. et al. Enhancing T cell therapy through TCR-signaling-responsive nanoparticle drug delivery. *Nat Biotechnol* **36**, 707-716 (2018).
15.   Pegram, H.J. et al. Tumor-targeted T cells modified to secrete IL-12 eradicate systemic tumors without need for prior conditioning. *Blood* **119**, 4133-4141 (2012).
16.   Rafiq, S. et al. Targeted delivery of a PD-1-blocking scFv by CAR-T cells enhances anti-tumor efficacy in vivo. *Nat Biotechnol* **36**, 847-856 (2018).
17.   Choi, B.D. et al. CAR-T cells secreting BiTEs circumvent antigen escape without detectable toxicity. *Nature Biotechnology* **37**, 1049-+ (2019).
18.   Zhang, L. et al. Tumor-infiltrating lymphocytes genetically engineered with an inducible gene encoding interleukin-12 for the immunotherapy of metastatic melanoma. *Clin Cancer Res* **21**, 2278-2288 (2015).

19. Zimmermann, K. et al. Design and Characterization of an "All-in-One" Lentiviral Vector System Combining Constitutive Anti-GD2 CAR Expression and Inducible Cytokines. *Cancers (Basel)* **12** (2020).

20. Kunert, A. et al. Intra-tumoral production of IL18, but not IL12, by TCR-engineered T cells is non-toxic and counteracts immune evasion of solid tumors. *Oncoimmunology* **7**, e1378842 (2017).

21. Roybal, K.T. et al. Precision Tumor Recognition by T Cells With Combinatorial Antigen-Sensing Circuits. *Cell* **164**, 770-779 (2016).

22. Kloss, C.C., Condomines, M., Cartellieri, M., Bachmann, M. & Sadelain, M. Combinatorial antigen recognition with balanced signaling promotes selective tumor eradication by engineered T cells. *Nat Biotechnol* **31**, 71-75 (2013).

23. Srivastava, S. et al. Logic-Gated ROR1 Chimeric Antigen Receptor Expression Rescues T Cell-Mediated Toxicity to Normal Tissues and Enables Selective Tumor Targeting. *Cancer Cell* **35**, 489-503 e488 (2019).

24. van Driel, W.J. et al. Hyperthermic Intraperitoneal Chemotherapy in Ovarian Cancer. *N Engl J Med* **378**, 230-240 (2018).

25. Chu, K.F. & Dupuy, D.E. Thermal ablation of tumours: biological mechanisms and advances in therapy. *Nat Rev Cancer* **14**, 199-208 (2014).

26. Mitchell, D. et al. A heterogeneous tissue model for treatment planning for magnetic resonance-guided laser interstitial thermal therapy. *Int J Hyperthermia* **34**, 943-952 (2018).

27. Lubner, M.G., Brace, C.L., Hinshaw, J.L. & Lee, F.T., Jr. Microwave tumor ablation: mechanism of action, clinical results, and devices. *J Vasc Interv Radiol* **21**, S192-203 (2010).

28. Amin, J., Ananthan, J. & Voellmy, R. Key features of heat shock regulatory elements. *Mol Cell Biol* **8**, 3761-3769 (1988).

29. Sakurai, H. & Enoki, Y. Novel aspects of heat shock factors: DNA recognition, chromatin modulation and gene expression. *FEBS J* **277**, 4140-4149 (2010).

30. Jaeger, A.M., Makley, L.N., Gestwicki, J.E. & Thiele, D.J. Genomic heat shock element sequences drive cooperative human heat shock factor 1 DNA binding and selectivity. *J Biol Chem* **289**, 30459-30469 (2014).

31. Whitlock, N.A., Agarwal, N., Ma, J.X. & Crosson, C.E. Hsp27 upregulation by HIF-1 signaling offers protection against retinal ischemia in rats. *Invest Ophthalmol Vis Sci* **46**, 1092-1098 (2005).

32. Wu, B.J., Kingston, R.E. & Morimoto, R.I. Human HSP70 promoter contains at least two distinct regulatory domains. *Proc Natl Acad Sci U S A* **83**, 629-633 (1986).

33. Kalmar, B. & Greensmith, L. Induction of heat shock proteins for protection against oxidative stress. *Adv Drug Deliv Rev* **61**, 310-318 (2009).

34. Vilaboa, N.E. et al. cAMP increasing agents prevent the stimulation of heat-shock protein 70 (HSP70) gene expression by cadmium chloride in human myeloid cell lines. *J Cell Sci* **108 (Pt 8)**, 2877-2883 (1995).

35. Xu, Q., Schett, G., Li, C., Hu, Y. & Wick, G. Mechanical stress-induced heat shock protein 70 expression in vascular smooth muscle cells is regulated by Rac and Ras small G proteins but not mitogen-activated protein kinases. *Circ Res* **86**, 1122-1128 (2000).

36. Kadonaga, J.T. Perspectives on the RNA polymerase II core promoter. *Wiley Interdiscip Rev Dev Biol* **1**, 40-51 (2012).

37. Flanagan, S.W., Ryan, A.J., Gisolfi, C.V. & Moseley, P.L. Tissue-specific HSP70 response in animals undergoing heat stress. *Am J Physiol* **268**, R28-32 (1995).

38. Klaassen, C.D., Liu, J. & Diwan, B.A. Metallothionein protection of cadmium toxicity. *Toxicol Appl Pharm* **238**, 215-220 (2009).

39. Safran, M. et al. Mouse model for noninvasive imaging of HIF prolyl hydroxylase activity: Assessment of an oral agent that stimulates erythropoietin production. *P Natl Acad Sci USA* **103**, 105-110 (2006).

40. Lokmic, Z., Musyoka, J., Hewitson, T.D. & Darby, I.A. Hypoxia and hypoxia signaling in tissue repair and fibrosis. *Int Rev Cell Mol Biol* **296**, 139-185 (2012).

41. Daugaard, M., Rohde, M. & Jaattela, M. The heat shock protein 70 family: Highly homologous proteins with overlapping and distinct functions. *FEBS Lett* **581**, 3702-3710 (2007).

42. Yamaguchi, M., Ito, A., Ono, A., Kawabe, Y. & Kamihira, M. Heat-inducible gene expression system by applying alternating magnetic field to magnetic nanoparticles. *Acs Synth Biol* **3**, 273-279 (2014).

43. Yin, P.T. et al. Stem cell-based gene therapy activated using magnetic hyperthermia to enhance the treatment of cancer. *Biomaterials* **81**, 46-57 (2016).

44. Nakatsuji, H. et al. Surface chemistry for cytosolic gene delivery and photothermal transgene expression by gold nanorods. *Sci Rep* **7**, 4694 (2017).

45. Gamboa, L. et al. Heat-Triggered Remote Control of CRISPR-dCas9 for Tunable Transcriptional Modulation. *ACS Chem Biol* **15**, 533-542 (2020).

46. Munoz-Sanchez, J. & Chanez-Cardenas, M.E. The use of cobalt chloride as a chemical hypoxia model. *J Appl Toxicol* **39**, 556-570 (2019).

47. Fotakis, G., Cemeli, E., Anderson, D. & Timbrell, J.A. Cadmium chloride-induced DNA and lysosomal damage in a hepatoma cell line. *Toxicol In Vitro* **19**, 481-489 (2005).

48. Mitchell, R.J. & Gu, M.B. Construction and characterization of novel dual stress-responsive bacterial biosensors. *Biosens Bioelectron* **19**, 977-985 (2004).

49. Phuagkhaopong, S. et al. Cadmium-induced IL-6 and IL-8 expression and release from astrocytes are mediated by MAPK and NF-kappaB pathways. *Neurotoxicology* **60**, 82-91 (2017).

50. Ede, C., Chen, X., Lin, M.Y. & Chen, Y.Y. Quantitative Analyses of Core Promoters Enable Precise Engineering of Regulated Gene Expression in Mammalian Cells. *Acs Synth Biol* **5**, 395-404 (2016).

51. Hansen, J. et al. Transplantation of prokaryotic two-component signaling pathways into mammalian cells. *Proc Natl Acad Sci U S A* **111**, 15705-15710 (2014).

52. Elias, D. et al. Optimization of hyperthermic intraperitoneal chemotherapy with oxaliplatin plus irinotecan at 43 degrees C after compete cytoreductive surgery: mortality and morbidity in 106 consecutive patients. *Ann Surg Oncol* **14**, 1818-1824 (2007).

53. Yang, X.J. et al. Cytoreductive surgery and hyperthermic intraperitoneal chemotherapy improves survival of patients with peritoneal carcinomatosis from gastric cancer: final results of a phase III randomized clinical trial. *Ann Surg Oncol* **18**, 1575-1581 (2011).

54. Nikfarjam, M., Muralidharan, V. & Christophi, C. Mechanisms of focal heat destruction of liver tumors. *J Surg Res* **127**, 208-223 (2005).

55. Hellevik, T. & Martinez-Zubiaurre, I. Radiotherapy and the tumor stroma: the importance of dose and fractionation. *Front Oncol* **4**, 1 (2014).

56. Miller, I.C., Gamboa Castro, M., Maenza, J., Weis, J.P. & Kwong, G.A. Remote Control of Mammalian Cells with Heat-Triggered Gene Switches and Photothermal Pulse Trains. *ACS Synth Biol* **7**, 1167-1173 (2018).

57. Chen, D.S. & Mellman, I. Oncology meets immunology: the cancer-immunity cycle. *Immunity* **39**, 1-10 (2013).

58. Mortier, E. et al. Soluble interleukin-15 receptor alpha (IL-15R alpha)-sushi as a selective and potent agonist of IL-15 action through IL-15R beta/gamma. Hyperagonist IL-15 x IL-15R alpha fusion proteins. *J Biol Chem* **281**, 1612-1619 (2006).

59. Robinson, T.O. & Schluns, K.S. The potential and promise of IL-15 in immuno-oncogenic therapies. *Immunol Lett* **190**, 159-168 (2017).

60. Rhode, P.R. et al. Comparison of the Superagonist Complex, ALT-803, to IL15 as Cancer Immunotherapeutics in Animal Models. *Cancer Immunol Res* **4**, 49-60 (2016).
61. Parihar, R. et al. NK Cells Expressing a Chimeric Activating Receptor Eliminate MDSCs and Rescue Impaired CAR-T Cell Activity against Solid Tumors. *Cancer Immunol Res* **7**, 363-375 (2019).
62. Steinbacher, J. et al. An Fc-optimized NKG2D-immunoglobulin G fusion protein for induction of natural killer cell reactivity against leukemia. *Int J Cancer* **136**, 1073-1084 (2015).
63. Xia, Y. et al. Treatment with a fusion protein of the extracellular domains of NKG2D to IL-15 retards colon cancer growth in mice. *J Immunother* **37**, 257-266 (2014).
64. Godbersen, C. et al. NKG2D Ligand-Targeted Bispecific T-Cell Engagers Lead to Robust Antitumor Activity against Diverse Human Tumors. *Mol Cancer Ther* **16**, 1335-1346 (2017).
65. Eagle, R.A., Jafferji, I. & Barrow, A.D. Beyond Stressed Self: Evidence for NKG2D Ligand Expression on Healthy Cells. *Curr Immunol Rev* **5**, 22-34 (2009).
66. Jain, P.K., Lee, K.S., El-Sayed, I.H. & El-Sayed, M.A. Calculated absorption and scattering properties of gold nanoparticles of different size, shape, and composition: applications in biological imaging and biomedicine. *J Phys Chem B* **110**, 7238-7248 (2006).
67. von Maltzahn, G. et al. Nanoparticles that communicate in vivo to amplify tumour targeting. *Nat Mater* **10**, 545-552 (2011).
68. von Maltzahn, G. et al. Computationally Guided Photothermal Tumor Therapy Using Long-Circulating Gold Nanorod Antennas. *Cancer Research* **69**, 3892-3900 (2009).
69. Lienert, F., Lohmueller, J.J., Garg, A. & Silver, P.A. Synthetic biology in mammalian cells: next generation research tools and therapeutics. *Nat Rev Mol Cell Biol* **15**, 95-107 (2014).
70. Fenno, L., Yizhar, O. & Deisseroth, K. The development and application of optogenetics. *Annu Rev Neurosci* **34**, 389-412 (2011).
71. Pan, Y. et al. Mechanogenetics for the remote and noninvasive control of cancer immunotherapy. *Proc Natl Acad Sci U S A* **115**, 992-997 (2018).
72. Piraner, D.I., Abedi, M.H., Moser, B.A., Lee-Gosselin, A. & Shapiro, M.G. Tunable thermal bioswitches for in vivo control of microbial therapeutics. *Nat Chem Biol* **13**, 75-80 (2017).
73. Evans, S.S., Repasky, E.A. & Fisher, D.T. Fever and the thermal regulation of immunity: the immune system feels the heat. *Nat Rev Immunol* **15**, 335-349 (2015).
74. Giavridis, T. et al. CAR T cell-induced cytokine release syndrome is mediated by macrophages and abated by IL-1 blockade. *Nat Med* **24**, 731-738 (2018).
75. Norelli, M. et al. Monocyte-derived IL-1 and IL-6 are differentially required for cytokine-release syndrome and neurotoxicity due to CAR T cells. *Nat Med* **24**, 739-748 (2018).
76. Leonard, J.P. et al. Effects of single-dose interleukin-12 exposure on interleukin-12-associated toxicity and interferon-gamma production. *Blood* **90**, 2541-2548 (1997).
77. Krishnamurthy, A. & Jimeno, A. Bispecific antibodies for cancer therapy: A review. *Pharmacol Ther* **185**, 122-134 (2018).
78. Bevilacqua, A., Fiorenza, M.T. & Mangia, F. A developmentally regulated GAGA box-binding factor and Sp1 are required for transcription of the hsp70.1 gene at the onset of mouse zygotic genome activation. *Development* **127**, 1541-1551 (2000).
79. Ramirez, V.P., Stamatis, M., Shmukler, A. & Aneskievich, B.J. Basal and stress-inducible expression of HSPA6 in human keratinocytes is regulated by negative and positive promoter regions. *Cell Stress Chaperones* **20**, 95-107 (2015).
80. Gaestel, M., Gotthardt, R. & Muller, T. Structure and organisation of a murine gene encoding small heat-shock protein Hsp25. *Gene* **128**, 279-283 (1993).
81. Miller, I.C., Castro, M.G., Maenza, J., Weis, J.P. & Kwong, G.A. Remote Control of Mammalian Cells with Heat-Triggered Gene Switches and Photothermal Pulse Trains. *Acs Synth Biol* **7**, 1167-1173 (2018).